Augmented Virtual Fluoroscopy for Minimally Invasive Diaphyseal Long Bone Fracture Reduction and Osteosynthesis

Guoyan Zheng, Xiao Dong, Xuan Zhang
MEM Research Center
University of Bern
Stauffacherstrasse 78
Bern, CH-3014, Switzerland
Guoyan.Zheng@MEMcenter.unibe.ch

Paul Alfred Grutzner
BG Trauma Center Ludwigshafen
University of Heidelberg
Ludwigshafen, Germany

ABSTRACT

This paper presents a novel technique to create an augmented virtual fluoroscopy for computer-assisted minimally invasive diaphyseal long bone fracture reduction. With this novel technique, repositioning of bone fragments during close fracture reduction and osteosynthesis will lead to image updates in each acquired imaging plane, which is equivalent to using several fluoroscopes simultaneously from different directions but without any X-ray radiation. The technique is achieved with a two-stage method. After acquiring a few (normally 2) calibrated fluoroscopic images and before fracture reduction, the first stage, *data preparation*, automatically identifies and segments the cylindrical bone fragments from the background in each image through a three-dimensional (3D) morphable object fitting process followed by a region information based active contour extraction. After that, the second stage, *image updates*, repositions the fragment projection onto each imaging plane during fracture reduction and osteosynthesis using an OpenGL based texture warping. Combined with photorealistic virtual implant model rendering technique, the present technique turns a close, indirect fracture reduction and osteosynthesis surgery in the real world into an open, direct one in the augmented virtual world. The technique has been successfully tested on phantom and *in vivo* experiments. Its application results in great reduction of the X-ray radiation to the patient as well as to the surgical team.

CR Categories: I.3.8 [Computer Graphics]: Applications; I.4.9 [Image Processing]: Applications; J.3.2 [Life and Medical Science]: Medical Information System;

Keywords: virtual fluoroscopy, computer-assisted surgery, fracture reduction, osteosynthesis, augmented reality

1 INTRODUCTION

Diaphyseal long bone fractures belong to the most common injuries encountered in clinical routine trauma surgery. Most of them are displaced and need to be surgically reduced. The past 15 years witnessed the shift from direct reduction and rigid fixation to biological internal fixation using indirect reduction techniques [1]. While in the past, fractures used to be exposed considerably and stabilized with accordingly sized plates, it is now generally agreed that the technique of minimally invasive osteosynthesis yields superior results. Minimization of the skin incision and reduction of the induced soft tissue damage results in a number of considerable advantages for the patient including both the cosmetic results as well as improvement in function and healing time [2].

One of the difficulties with minimally invasive techniques in fracture treatment is caused by the absence of direct visual contact to fracture reduction and implant positioning. As a consequence, the fluoroscope, also known as C-arm, is used more intensively during modern surgical techniques for visualizing underlying bone, implant, and surgical tool positions. The disadvantages of fluoroscope include two-dimensional (2D) projection image from single view, limited field view, distorted images, and last but not least, high radiations to both the patient and the surgical team [3]. The integration of conventional fluoroscopes into computer assisted navigation systems has been established as one means to overcome certain of these drawbacks [4][5][6][7][8][9].

Fluoroscopy-based navigation systems try to intrinsically and extrinsically calibrate fluoroscopes to compensate for their distortions and to create a virtual fluoroscopy, which provides the missing link between intra-operative imaging information of the surgical reality with the surgical action for different surgical applications [9]. The one specific application area is long bone fractures, especially diaphyseal long bone fracture reduction. In [5] static fluoroscopic images was replaced with a virtual display of 3D long bone models created from pre-operative Computed Tomography (CT) and tracked intra-operatively in real time. Fluoroscopic images were used to register the bone models to the intra-operative situation [10]. In [7] a computer-assisted fluoroscopy-based navigation system for reduction of femoral fracture and antetorsion correction was developed. In this system, the bone fragments were represented by their individual axes and alignment of bone fragments during fracture reduction was monitored through real-time visualization of line graphics. Bi-planar landmark reconstruction was proposed to contactlessly determine the coordinates of deep-seated landmarks. A patient-specific coordinate system was then established based on these reconstructed landmarks for measuring changes of leg length and antetorsion. Recently we have proposed to enhance this system using a 3D cylindrical model representation of each bone fragments, which is interactively reconstructed from the acquired fluoroscopic images [11].

Although a number of authors reported excellent experiences in restoration of leg lengths and antetorsion for diaphyseal long bone fracture reduction with currently existing systems for virtual fluoroscopy [12][13], two disadvantages of these devices can be identified during routine clinical use: (1) the bone fragments were represented either by simple 3D models (lines or cylinders) interactively reconstructed from the acquired fluoroscopic images or by complex surface models constructed from pre-operative CT data. The former represents the surgical reality in a rather abstract way and the latter requires a pre-operative CT data, which adds financial burden and radiation to the patient; (2) changes in the bony anatomy due to fracture reduction can only be analyzed by the re-acquisition of C-arm images causing additional radiation to

patient and surgical staff and requiring cumbersome re-positioning of the fluoroscope at the patient during surgery.

To address these issues, we have developed a novel technique to create an augmented virtual fluoroscopy for computer-assisted minimally invasive diaphyseal long bone fracture reduction and osteosynthesis. With this novel technique, repositioning of bone fragments during fracture reduction will lead to image updates in each acquired imaging plane, which is equivalent to using several fluoroscopes simultaneously from different directions but without any X-ray radiation. Combined with photorealistic virtual implant model rendering technique, this novel technique turns a close fracture reduction and osteosynthesis surgery in the real world into an open one in the augmented virtual world.

This paper is organized as follows. Section 2 presents the image calibration method. Algorithm for automated detection and segmentation of bone fragments is described in Section 3. Details about how to achieve augmented virtual fluoroscopy is given in Section 4. Section 5 presents our experimental results followed by discussions and conclusion in Section 6.

2 IMAGE CALIBRATION

Real-time navigation is achieved through rigid-body coordinate transformations based on optoelectronic tracking (OPTOTRAK 3020; Northern Digital, Ontario, Canada) of the C-arm, the bone fragments, and surgical tools. For this purpose, optoelectronically trackable marker shields containing infrared (IR) light-emitting diodes (LEDs) are attached to the C-arm, each bone fragment, and surgical tool. The LEDs on each shield define local coordinate systems (COS) with a fixed relation to every point on the assigned rigid body. The role of the optoelectronic tracker is to provide matrices $T_{X,Y}$ that allow coordinate transformations from any involved **X-COS** to **Y-COS**.

In the following description, let's denote DRB_{Fi} as the dynamic reference base (DRB) attached to the ith trackable fragment F_i, i = 1, 2, . . . ,N_F , and the local coordinate system defined by DRB_{Fi} as $DCOS_{Fi}$. Several (typically 2) C-arm images $S = \{S_k, k = 1, 2, \ldots, N_S\}$ are then acquired from different view directions, as shown in Figure 1. Further denote the local reference coordinate system in each C-arm shot S_k as $CCOS_k$, the transformations $T_{i,k}$ between $DCOS_{Fi}$ and $CCOS_k$ at the acquisition time of each C-arm shot can be obtained and recorded, which are used to co-register the N_S independent C-arm images to a chosen reference coordinate system $DCOS_{Fi}$. Without causing confusion, in this section we denote this chosen patient reference coordinate system as *A-COS*.

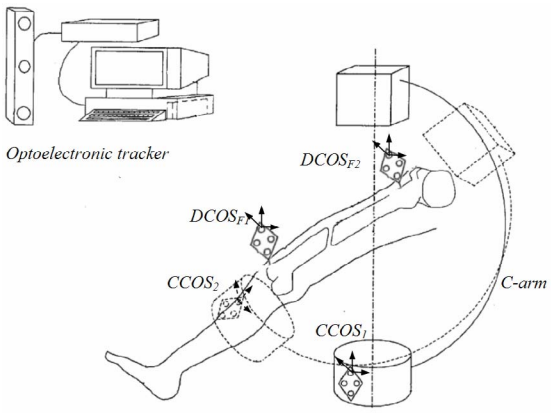

Figure 1. Schematic view of image acquisition for fluoroscopy based navigation of long bone fracture reduction and osteosynthesis

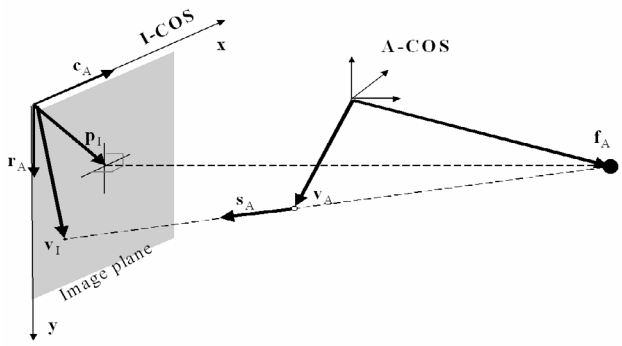

Figure 2. Weak-perspective pin-hole camera model

To relate a pixel in the two-dimensional (2D) projection image to *A-COS*, the acquired image has to be calibrated for physical projection properties and be corrected for various types of distortion. In a previously published paper [6] from our institution, a weak-perspective pin-hole camera model, as shown in Figure 2, was chosen for modelling the C-arm projection. Using such a camera model, a 2D pixel $\mathbf{V_I}$ is related to a three-dimensional (3D) point $\mathbf{V_A}$ by following equations [6]:

$$\mathbf{S_A} = \frac{(\mathbf{V_A} - \mathbf{f_A})}{\|\mathbf{V_A} - \mathbf{f_A}\|};$$

$$\begin{bmatrix} V_{I,x} \\ V_{I,y} \\ 1 \end{bmatrix} = \begin{bmatrix} c_{A,x} & c_{A,y} & c_{A,z} & p_{I,x} \\ r_{A,x} & r_{A,y} & r_{A,z} & p_{I,y} \\ 0 & 0 & 0 & 1 \end{bmatrix} \begin{bmatrix} S_{A,x} \\ S_{A,y} \\ S_{A,z} \\ 1 \end{bmatrix} \quad (1)$$

where $\|\cdot\|$ means to calculate the length of a vector and the vectors $\mathbf{f_A}$, $\mathbf{r_A}$, $\mathbf{c_A}$ and $\mathbf{p_I}$ represent the position of focal point, the vector along image row increasing direction, the vector along image column increasing direction, and the 2D position of piercing point, respectively. They are projection parameters used to describe the projection properties of the C-arm and need to be calibrated preoperatively.

Eq. (**1**) can be used for both forward and backward projections. For example, if we want to calculate the direction $\mathbf{S_A}$ of the forward projection ray of a pixel $\mathbf{V_I}$, an additional constraint $\|\mathbf{S_A}\| = 1$ can be used together with Eq. (**1**) to solve for it. The forward projection ray of point $\mathbf{V_I}$ is defined by the focal point and the direction $\mathbf{S_A}$.

The position of the imaging plane in *A-COS* and the focal length in our camera model is implicitly determined using the calibrated focal point $\mathbf{f_A}$ and the vectors $\mathbf{r_A}$ and $\mathbf{c_A}$. Any 2D image pixel $\mathbf{V_I}$ corresponds to a 3D spatial point $\mathbf{I_A}$ on this imaging plane, which is the intersection point between its forward projection ray and this imaging plane.

3 AUTOMATED DETECTION AND SEGMENTATION OF BONE FRAGMENTS

3.1 Image Feature Extraction

A Canny Edge Detector [14] is applied to all the C-arm images and the "raw" edge images can then be obtained. Due to the complex background and varieties of feature types, the "raw" edge data is a combination of the true bone shaft edges, and the

false edges from attached instruments, cables, external fixator, image noise, and fractural sites. A simple thresholding on the intensity distribution in the neighborhood of the detected edge points is used to partially eliminate undesired false edges from metal instruments. Then for each fractural fragment F_i, there exists a correspondent edge point set $E_{Fi} = \{E_{kFi}, k = 1, \ldots\ldots, N_S\}$, where E_{kFi} is the edge point set in C-arm image S_k that belongs to fragment F_i.

3.2 Morphable Model Fitting for Fragment Detection

Let's assume that the cylindrical fragment F_i is modelled as a cylinder C_{Fi}. The cylinder can be parameterized with parameter $[r_{Fi}, p_{Fi}]$, where r_{Fi}, and $p_{Fi} = [x_{Fi}, y_{Fi}, z_{Fi}, \alpha_{Fi}, \beta_{Fi}, \gamma_{Fi}]$ are the radius and 6 degree of freedom pose of the cylinder in $DCOS_{Fi}$, respectively. Therefore the identification and pose/size estimation of fragments can be regarded as an optimal process for fitting 3D parameterized model to images [15][16][17]. But instead of directly applying the well-known optimization techniques such as Newton-type optimization method [15] or Levenberg-Marqardt non-linear optimization algorithm [16] to find out the parameters $[r_{Fi}, p_{Fi}]$ for C_{Fi}, we can convert our optimization problem into an iterative closest point matching problem in 3D [17], (see Figure 3.), which is iteratively solved as follows.

Algorithm for fragment detection

The following two steps iterate until parameter values converge:

- Denote the current configuration of C_{Fi} at time t as $[r_{Fi}^{(t)}, p_{Fi}^{(t)}]$, for each edge point e_{kFi}^m in E_{kFi}, we calculate the point pair $PP_{kFi}^m = (P_{kFi}^{me}, P_{KFi}^{mc})$, where P_{kFi}^{me} and P_{KFi}^{mc} are the two points on the back-projection line of e_{kFi}^m and on the surface of C_{Fi}, respectively, and give the shortest distance, as shown in Figure 3. Then, the overall probability of which the detected edge points $\{e_{kFi}^m\}$ are from the projection boundary of the cylinder model $[r_{Fi}^{(t)}, p_{Fi}^{(t)}]$ could be represented as $\prod_m (e^{-|d(BP_{kFi}^m, C_{Fi}(r_{Fi}^{(t)}, p_{Fi}^{(t)})) - r_{Fi}^{(t)}|^2})$, or equivalently as $\prod_m (e^{-|P_{kFi}^{me} - P_{KFi}^{mc}|^2})$.
- In this step, we try to maximize the probability $\prod_m (e^{-|d(BP_{kFi}^m, C_{Fi}(r_{Fi}^{(t)}, p_{Fi}^{(t)})) - r_{Fi}^{(t)}|^2})$, given the cylinder model configuration $[r_{Fi}^{(t)}, p_{Fi}^{(t)}]$. It is equivalent to apply a paired-point matching algorithm to the paired-pint set $PPS_{Fi}^{(t)} = \{PP_{kFi}^m\}$ to obtain a rigid registration transformation $T_{Fi}^{(t)}$; then update the pose $p_{Fi}^{(t+1)}$ of C_{Fi} by $T_{Fi}^{(t)}$; and further update $r_{Fi}^{(t+1)}$ as the average distance between the back-projection line of e_{kFi}^m and the axis of C_{Fi} using the updated pose $p_{Fi}^{(t+1)}$.

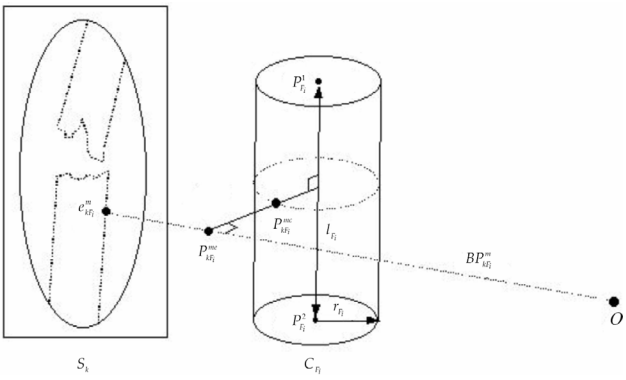

Figure 3. Converting a model fitting problem to an iterative closest paired point matching problem; *O* is the focal point of calibrated C-arm image S_k

3.3 RANSAC-based Morphable Model Fitting for Robust Fragment Detection

Outliers exist even after eliminating the false edge points from metal instruments. Without further elimination procedure, even a small number of outliers may greatly influence the result of fragment pose/size estimation, especially under an improper initialization of C_{Fi}. In our method this is handled using the Random Sample Consensus (RANSAC) paradigm [18]. Each time a certain percentage (e.g. 20%) of edge points are randomly sampled from E_{Fi}; the algorithm described in last sub-section is applied to calculate an optimal solution using those sampled edge points; the number of edge points in E_{Fi} which satisfy $d(BP_{kFi}^m, C_{F_i}(r_{F_i}, p_{F_i})) \approx r_{Fi}$ are recorded as M. This procedure is repeated a fixed number of times (e.g. 200 times) and the $[r_{Fi}, p_{Fi}]$ that yields the largest M is selected as the final estimation.

3.4 Fragment Contour Extraction

In this step, a region-based active contour with local depth adapting algorithm [19] is implemented to segment the fragment contours based on the result of fragment pose/size estimation. The initial position of the contour is set as the outer projection boundary of the estimated cylinder on a C-arm shot. Usually the outer projection boundary is not far from the true fragment contour; therefore the algorithm needs only a few iterations before its convergence.

4 Augmented Virtual Fluoroscopy with Zero-Dose Image Updates

4.1 Overview

The augmented virtual fluoroscopy with zero-dose image updates for minimally invasive diaphyseal long bone fracture reduction is achieved with a two-stage procedure, as shown in Figure 4. Starting from a few (normally 2) acquired fluoroscopic images before fracture reduction, the first stage, *data preparation*, tries to prepare necessary data for the second stage. The second stage, *image updates*, then repositions the fragment projection in each acquired image during fracture reduction and osteosynthesis an OpenGL based texture warping, which is equivalent to using several fluoroscopes simultaneously from different directions but without any X-ray radiation. The details of these two stages are described below.

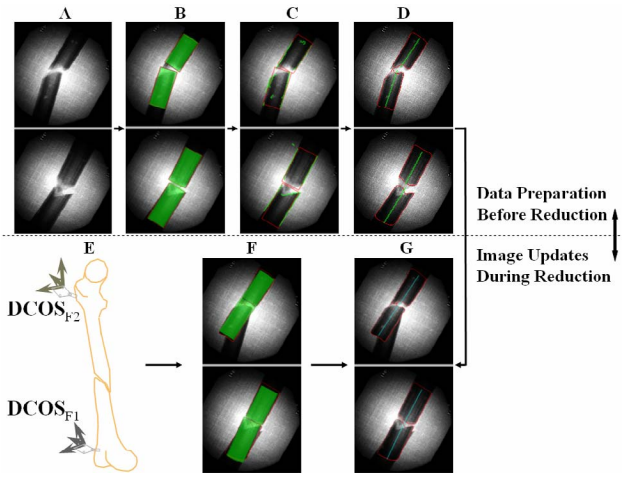

Figure 4. Overview of the algorithms for achieving computerized fluoroscopy with zero-dose image updates

4.2 Data Preparation

The tasks of this step include: A. image acquisition; B. automated fragment identification, pose and size estimation; C. fragment projection contour extraction; and D. interpolation weights computation for each diaphyseal bone fragments of femur, as shown by the first row of Figure 4. The algorithm described in Section 3 is used to automatically detect bone fragment from complex background. The detected main fragments are presented as green cylindrical models in sub-figure B of Figure 4. The projection of each identified cylinder onto into imaging plane, a quadrilateral (see sub-figure C of Figure 4), is then fed to a region information based active contour model [19] to extract the fragment projection contour (see sub-figure D of Figure 4). And for each point on the contour, four interpolation weights relative to the four vertexes of the cylinder projection are calculated as follows, which completes the data preparation step.

Let's denote the four vertices of the cylinder projection as $P_0=(x_0,y_0)$, $P_1=(x_1,y_1)$, $P_2=(x_2,y_2)$, $P_3=(x_3,y_3)$, which define a quadrilateral. Any point $P=(x,y)$ inside this quadrilateral can be interpolated by its four vertices using following equations:

$$P=\sum_{i=0}^{3} W_i \cdot P_i \quad and \quad \begin{cases} W_0=(1-r)\cdot(1-s) \\ W_1=r\cdot(1-s) \\ W_2=r\cdot s \\ W_3=(1-r)\cdot s \end{cases} \qquad (2)$$

where W_i is the interpolation coefficients for P_i.

To further calculate the parametric coefficients (r,s), a Newton-type downhill iterative optimization algorithm is used by reformulating the problem as:

$$\begin{cases} f(r,s)=x-\sum_{i=0}^{3} W_i \cdot x_i = 0 \\ g(r,s)=y-\sum_{i=0}^{3} W_i \cdot y_i = 0 \end{cases} \qquad (3)$$

4.3 Image Updates

This step starts with interpolation of the new position of each point on the fragment projection contour using the interpolation coefficients calculated in the first stage and the new position of the corresponding quadrilateral. The position of the vertices of the quadrilateral is updated in real time according to the positional changes of the associated bone fragments, as determined by the navigation system during fracture reduction and osteosynthesis (see step F of Figure 4). The newly calculated image coordinates of the fragment projection contour are then fed to an OpenGL® based texture warping pipeline [20] to achieve a real-time image updates, as shown by sub-figure G of Figure 4.

5 Experimental Results

5.1 Phantom Experimental Results

We performed experiment to evaluate the effectiveness of the proposed technique. Images of the plastic femur with simulated fracture were used for this experiment. To simulate a realistic situation, the field of views of those input images contain not only projections from bone fragment but also those from cables and DRB fixation devices, as shown in Figure 5-A. The "raw" edges extracted by an edge detector are presented in Figure 5-B. Figure 5-C shows the optimally estimated cylinders together with their outer projection boundaries (red quadrilaterals) and Figure 5-D presents the segmentation results. Finally, Figure 5-E shows the image updates by the proposed technique, when the fracture is reduced. The repositioned fragment projections in this image are highlighted by their surrounding contours and their axes.

5.2 In vivo Experimental Results

The LISS® (Stratec-Medical, Oberdorf, Switzerland) is an osteosynthesis system allowing for the minimally invasive fixation of problematic metaphyseal fractures with angular stabilization. In a sense, it is comparable to an internal fixator. However, its implantation is challenging and usually does not allow any errors. The implant has to fit the convexity of the bone precisely.

After successful laboratory evaluation, the present augmented virtual fluoroscopy technique was integrated into the existing navigation system. This technology was then applied during osteosynthesis supported by LISS. A consecutive case study of three patients with four fractures of the proximal tibia was performed.

The surgical procedure was as follows. First, DRBs were fixed to the proximal and distal main fragments. Fluoroscopic images were acquired in two different planes, both proximally and distally of the fractures, as well as at the levels of the fractures. Subsequently, the fractures were reduced and fixed with navigational support (Figure 6, A and B). With the help of the present augmented virtual fluoroscopy technique, the entire procedure could be carried out without additional fluoroscopic checking. Owing to the interactive feedback of the displayed and the tactile information during surgery, the reduction could be performed in all cases in a simple and fast manner. In real time, the LISS plates, the drill, and the screw driver with the attached screws were visualized photo-realistically in their correct spatial relation to the acquired images (see Figure 7 for the comparison the real X-ray projection and the virtual plate visualization). The insertion of the plates, as well as the subsequent fixation procedure including drilling, depth measurement, and screw insertion, could be navigated without any further radiation exposure.

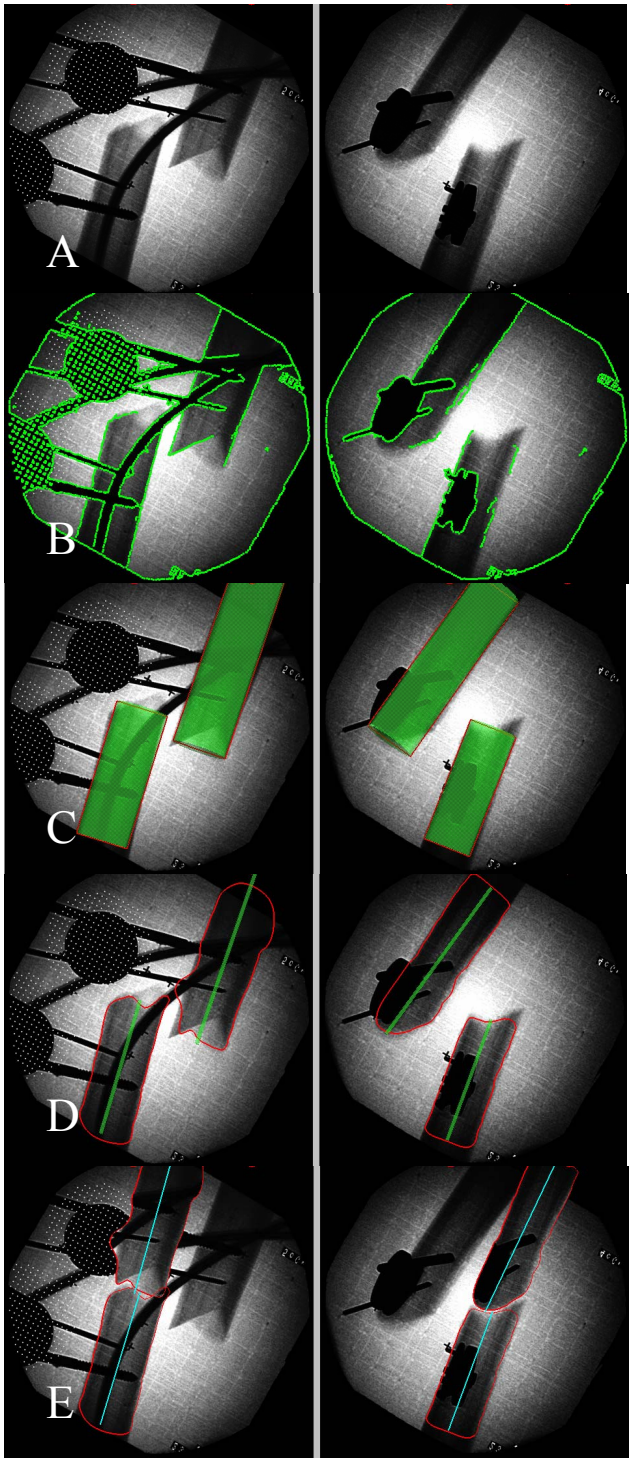

Figure 5. Complete procedure of computerized fluoroscopy with zero-dose image updates for minimally invasive femoral diaphyseal fracture reduction. (A) input images; (B) edge pixels extraction; (C) bone fragment detection; (D) contour extraction; (E) image updates.

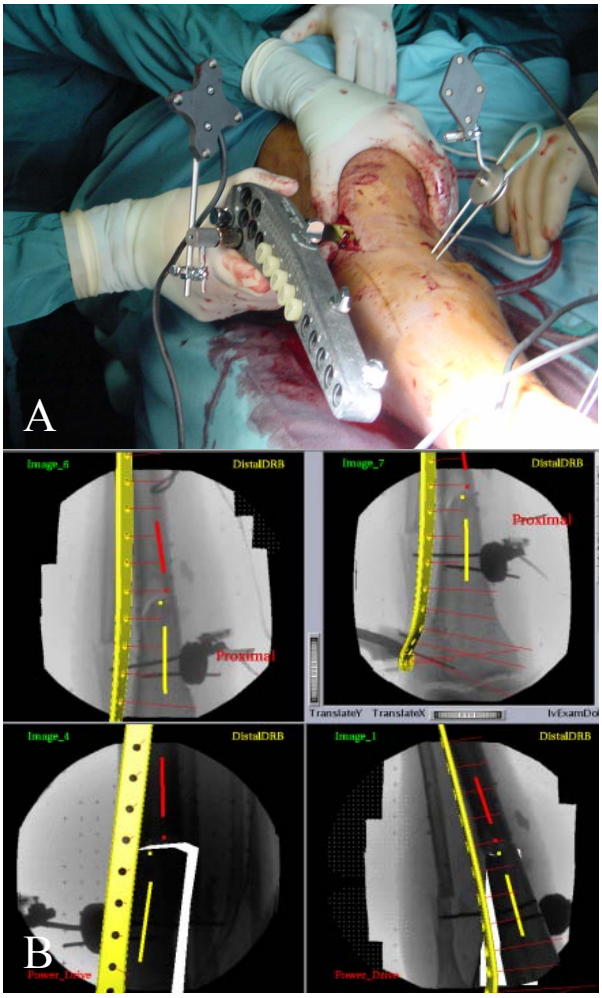

Figure 6. Reality augmented virtual fluoroscopy for the intraoperative monitoring of fracture reduction and osteosynthesis fixation. (A) Intraoperative surgical situs (plate insertion); (B) the corresponding reality augmented virtual fluoroscopy

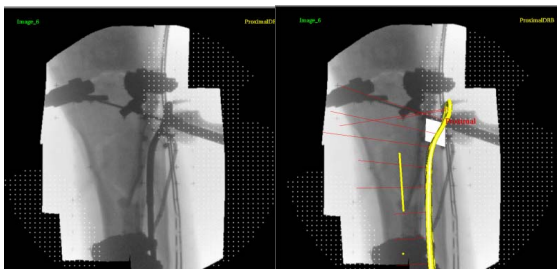

Figure 7. Intraoperative verification images. Note that a perfect matching between the real X-ray projection shown in left image and the virtual projection shown in right image was observed

6 Discussions and Conclusions

The persisting problem in minimally invasive fracture reduction is related to the precise and atraumatic reduction of the main fragments. The repetitive checking of reduction during surgery and interference between reduction and the fixation of implants are the most demanding and time-consuming elements. The aims of the present technique were to provide radiation-free control mechanisms during fracture reduction by navigated C-arm images (virtual fluoroscopy) and to represent implants and instruments photo-realistically to overcome the aforementioned difficulties. There is no need for preoperative planning steps such as image processing or interactive definition of anatomical landmarks. The system does not require the intraoperative registration of preoperative image data (matching) as is mandatory for CT-based navigation. Another advantage of virtual fluoroscopy is the ability to update the navigational image data at any time, which may become necessary after changes to the anatomical situation owing to fracture reduction maneuvers or osteotomies.

The proposed augmented virtual fluoroscopy technique, combined with the photorealistic visualization technique, provides the surgeon with 3D visualization of osteosynthesis implants and offers several advantages: It allows the simultaneous display of several views of the fractured bone during reduction, and it is possible to visualize the fracture, including axial, rotational, and length alignment, from any viewpoint. With this reality-augmented navigation system, a close, indirect reduction in the real world has been turned into an open, direct reduction in the virtual world. This allows the control of instruments through direct insight into the virtual world. And for the first time, radiation-free updates of fluoroscopic images are possible, which considerably decreased the radiation exposure to the patient as well as to the surgical team.

References

[1] M. Leunig, R. Hertel, K.A. Siebenrock, et al. The evolution of indirect reduction techniques in the treatment of fractures. Clin Orthop, vol. 375, pp. 7-14, 2000

[2] C. Krettek, T. Gerich, and T. Miclau. A minimally invasive medial approach for proximal tibial fractures. Injury, vol. 32 Suppl 1, pp. S4-S13, 2001

[3] Y.R. Yampersaud, K.T. Foley, A.C. Shen, S. Williams, and M. Solomito. Radiation exposure to the spine surgeon during fluoroscopially assisted pedicle screw insertion. Spine, vol. 25, pp. 2637-2645, 2000.

[4] R. Hofstetter, R. Slomczykowski, I. Bourquin, L.-P. Nolte. Fluoroscopy based surgical navigation – concept and clinical applications. Proceedings of the 11th International Symposium on Computer Assisted Radiology and Surgery, pp. 956 – 960, 1997

[5] L. Joskowicz, C. Milgrom, A. Simkin, et al. FRACAS: a system for computer-aided image-guided long bone fracture surgery. Comp Aid Surg, vol. 3, pp. 277-288, 1998

[6] R. Hofstetter, M. Slomczykowski, M. Sati, L.-P. Note. Fluoroscopy as an image means for computer-assisted surgical navigation. Comp Aid Surg, vol. 4, pp. 65-76, 1999

[7] R. Hofstette, M. Slomczykowski, C. Krettek, et al. Computer-assisted fluoroscopy-based reduction of femoral fractures and antetortion correction. Comp Aid Surg, vol. 4, pp. 311-325, 2000

[8] L.-P. Nolte, M.A. Slomczykowski, U. Berlemann, M. J. Matthias, R. Hofstetter, D. Schlenzka, T. Laine, and T. Lund. A new approach to computer-aided spine surgery: fluoroscopy-based surgical navigation. Eur Spine J, vol. 9 Suppl, pp. S78 – S88, 2000

[9] K. Foley, D. Simon, Y.R. Rampersaud. Virtual fluoroscopy: Computer-assisted fluoroscopic navigation. Spine, vol. 26 pp. 347-351, 2001

[10] H. Livyatan, Z. Yaniv, and L. Joskowicz. Gradient-based 2-D/3-D Rigid Registration of Fluoroscopic X-ray to CT. IEEE T Med Imaging, Vol. 22, No. 11, pp. 1395 – 1406, 2003

[11] P.A. Grutzner, G. Zheng, B. Vock, C. Keil, L.-P. Nolte, A. Wentzensen. Computer-assisted osteosynthesis of long bone fracture. In Navigation and Robotics in Total Joint and Spine Surgery. J.B. Stiehl, W. Konermann, R. Haaker, (eds), Springer-Verlag: 449-454, 2003.

[12] N. Suhm, A.L. Jacob, L.-P. Nolte, P. Regazzoni, and P. Messmer. Surgical navigation based on fluoroscopy – clinical application for computer-assisted distal locking of intramedullary implants. Comp Aid Surg, vol. 5, pp. 391-400, 2000

[13] M.A. Slomczykowski, R. Hofstetter, M. Sati, C. Krettek, and L.-P. Nolte. Novel computer-assisted fluoroscopy system for intraoperative guidance: feasibility study for distal locking of femoral nails. J Orthop Trauma, vol. 15, pp. 122-131, 2001

[14] J. Canny. A Computational Approach to Edge Detection. IEEE T Pattern Anal, vol. 8, pp. 679-698,1986.

[15] D.G. Lowe. Fitting parameterized three-dimensional models to images. IEEE T Pattern Anal, vol. 13, pp. 441-450, 1999

[16] A. Pece, A. Worrall. A Newton method for pose refinement of 3D models. Proceedings of the 6th Int. Symposium on Intelligent Robotic System, Edinburgh, UK, July 1998.

[17] A. Guéziec, P. Kazanzides, B, Williamson and R. Taylor. Anatomy-Based Registration of CT-scan and Intraoperative X-ray Images for Guiding a Surgical Robot. IEEE T Med Imaging, Vol. 17, No. 5, pp. , 715 – 728, 1998.

[18] M.A. Fischler and R.C. Bolles. Random sample consensus: a paradigm for model fitting with applications to image analysis and automated cartography. Commun. ACM, vol 24, pp. 381-395, 1981

[19] R. Ronfard. Region-based strategies for active contour models. International Journal of Computer Vision, vol. 13, pp. 229-251, 1994

[20] J. Neider, T. Davis, M. Woo. OpenGL Programming Guide. Second edition, Addison-Wesley Publishing Company, 1997